RSC Advances

ROYAL SOCIETY OF CHEMISTRY

www.rsc.org/advances

RCS Advances

ARTICLE

Design of a polypyrrole MIP-SAW sensor for selective detection of flumequine in aqueous media. Correlation between experimental results and DFT calculations

N. Ktari,[a] N. Fourati,[b,1] C. Zerrouki,[b] M. Ruan,[c,d] M. Seydou,[c] F. Barbaut,[c] F. Nal,[e] N. Yaakoubi[f], M. M. Chehimi,[c,g] and R. Kalfat[a]

Received 00th January 20xx,
Accepted 00th January 20xx

DOI: 10.1039/x0xx00000x

www.rsc.org/

Abstract: A shear horizontal surface acoustic wave sensor (SH-SAW) operating at 104 MHz was functionalized with a polypyrrole (PPy) molecularly imprinted polymer (MIP) for selective detection of flumequine (FLU) in aqueous media. In order to prevent the formation of FLU complexes with the gold sensing area of the SH-SAW sensor, a thin blocking polypyrrole layer was deposited by chronoamperometry before the MIP electrochemical deposition. The detection limit of the designed sensor was of order of 1 μM and the sensitivity was estimated to be at 9.36 ± 0.39 °/mM. Selectivity tests were made with levofloxacin (LEVO), an interfering fluoroquinolone antibiotic. Results indicate that the designed PPy-MIP recognition layer is selective of flumequine. Quantum chemical calculations, based on the density functional theory (DFT), have permitted to highlight the importance of the PPy blocking layer, on the one hand, and the nature of interactions between the polypyrrole matrix and FLU and LEVO analytes, on the other hand.

1 Introduction

The rapid growth of industrial aquaculture has been accompanied by an important use of antibiotics in rivers, lakes and oceans[1-4]. It has been demonstrated that, 70-80 % of drugs administered as fish medicated feed, during a treatment period, ends up into the environment[5]. Thus, concerns have emerged about serious problems induced by these residues on human health, such as the development of antibiotic-resistant bacteria or allergic reactions.

Flumequine (FLU) is a fluoroquinolone (FQs) antibiotic usually used in intensive aquaculture[6, 7]. It is quite persistent (approximately 150 days half-life in surface sediment[5]), and has been found in the wastewater of a sea bass intensive aquaculture station, after 5-day oral treatment, at levels of 3. 10^{-4} M [7]. Owing to their extensive use, the residuals of the fluoroquinolone antibiotics may remain not only in fish tissues, but also in bass water. Nevertheless, there is a lack of legislation regarding tolerance levels of this veterinary drug in natural waters[8]. Chromatographic techniques like HPLC (High-Performance Liquid Chromatography)[9], HPLC-MS (High-Performance Liquid Chromatography-Mass Spectrometry)[10-11] or

[a] *Laboratoire Méthodes et Techniques d'Analyse, INRAP, BiotechPole, 2020, Sidi-Thabet, Tunisia*
[b] *Cnam, SATIE, UMR CNRS 8029 ENS Cachan-Cnam, 292 rue Saint Martin, 75003, Paris, France*
[c] *Université Paris Sorbonne Paris Cité, ITODYS, UMR 7086, CNRS 15 rue J-A de Baïf, 75013, Paris, France*
[d] *School of Materials and Metallurgy, Hubei Polytechnic University, Huangshi, Hubei, China*
[e] *EP AnaPhy/Physique, Cnam, 292 rue Saint Martin, 75003 Paris, France*
[f] *Université du Maine, LAUM, UMR CNRS 6613, Avenue Olivier Messiaen 72085 LE MANS Cedex9*
[g] *Université Paris-Est Créteil, CNRS UMR 7182 ICMPE, 2-8 rue Henri Dunant, 94320 Thiais, France*
[1] *Corresponding author. Email: fourati@cnam.fr*
Tel. + 33 1 58 80 87 03, Fax. + 33 1 40 27 29 54

more recent pCEC (Pressurized Capillary Electrochromatography)[12] are generally used for the determination of fluoroquinolones in different matrixes including milk, eggs, butter, chicken, ovine, porcine kidney and fish muscles. Other studies have reported coupling of HPLC with optical detection, such as fluorescence[13-14] or UV[15] ones. Despite their reliability, high sensitivity and low detection limits, chromatographic techniques present some limitations, related to their high cost and analysis time, and some other inherent problems like solvent composition and flow rate[16]. Other devices like enzyme-linked immunosorbent assays (ELISA)[17-18] and microbiological assays[19] have been also described. In recent years, several SPR immunosensors[20-21] have been developed for detecting low levels of fluoroquinolone residues. Despite their inherent advantages, the high cost and the poor physicochemical stability of the antibodies or enzymes prevent their use in routine analysis.

In the present study, we report the use of a surface acoustic wave (SAW) sensor to follow-up flumequine extraction and its further recognition. These devices have been used to detect either chemical or biological analytes, due to their selectivity, sensitivity, reliability and low limits of detection (LOD)[22-24]. As a functional layer, we have electrosynthesized a biomimetic polypyrrole receptor for flumequine that is a thin flumequine imprinted polypyrrole.

The rationale for preparing molecularly imprinted polymers (MIPs) is that they are easy to prepare, stable, cheap, selective, and can be used in extreme environments, such as highly charged media[25-29]. Moreover, MIPs can be prepared by electropolymerization directly on the sensing part of a transducer[30-32]. Interestingly, the polymer is deposited onto an electrode surface and its formation is controlled by varying the polymerization conditions, such as the deposition time, the applied potential or the bath concentration[33].

In this work, we have chosen polypyrrole (PPy) as matrix, among the large variety of polymers for electrosynthesized MIPs[31,33-35]. The creation of imprinted sites within PPy is based on the irreversible overoxidation which may result in the incorporation of carbonyl and carboxylic groups into the polypyrrole backbone[33,36]. The selectivity of the designed MIP-SAW senor was investigated by examining the gravimetric responses in presence of levofloxacin (LEVO), an interfering fluoroquinolone antibiotic which is considered as one of the most potent antibacterial agents on the market and the most prescribed quinolone class antibiotic worldwide[37,38].

By using theoretical calculations based on density functional theory (DFT), we assess conformational and chemical complementarity between the FLU template and functional entities (from simple monomer to tetramer). The complexes were fully optimized with appropriate hybrid functional, and the interaction energies (ΔE) were determined for the optimized structures. As mentioned in previous work [23], here also, we showed that it is necessary to weight the computed interaction energies per molecular volume to take into account the porous character of MIPs.

Our literature survey on the detection of flumequine or any other related fluoroquinolones by surface acoustic wave sensors functionalized with thin conductive polymers has not been reported previously, hence the motivation for this work.

2 Experimental

2.1 Chemicals

Pyrrole, tetra-fluoro-ammonium-tetra-fluoroborate ($tBuNBF_4$), flumequine (FLU), levofloxacin (LEVO) anhydrous quality acetonitrile (ACN), methanol (MeOH), acetic acid (AcCOOH) H_2SO_4 (95%) and H_2O_2 (30%) were purchased from Sigma Aldrich. Pyrrole was purified before its use by filtering through basic alumina column and stored in dark at 4°C.

$tBuNBF_4$ was used as supporting electrolyte for electrochemical measurements. Flumequine and levofloxacin were used as received.

2.2 Instrumentation

2.2.1 Gravimetric measurements

The developed gravimetric sensor is a shear horizontal surface acoustic wave device fabricated on 36°rot lithium tantalate substrate. The operating frequency is of about 104 MHz. The sensitive area and interdigital transducer electrodes were realized by evaporation of (20/80) nm Cr/Au layers. The measurement setup consists of a PPy-MIP-coated SAW sensor, a Kalrez® flow cell, deposited on the sensing region, a PMMA cover including inlets and outlets (Fig 1), a peristaltic pump, and a homemade pulse mode system to monitor phase output versus time at a fixed frequency.

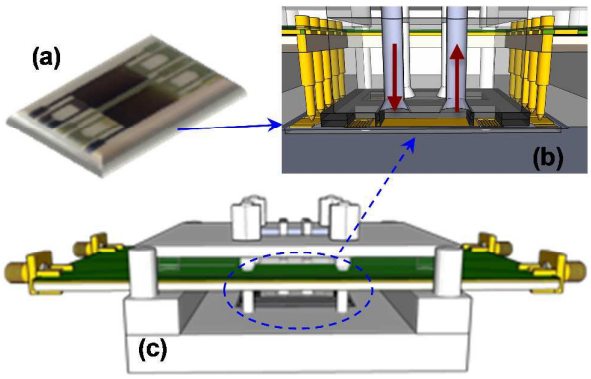

Fig 1 Schematic representation of a part of the SAW sensor's setup:
(a) PPy-MIP-coated SAW sensor, (b) a sectional view
(c) complete assembly including the printed circuit board

2.2.2 Electrochemical measurements

Cyclic voltammetry and amperometric measurements were carried out using potentiostat/galvanostat PG581 apparatus interfaced with PG581software. A conventional three-electrodes system in one compartment cell was used with a steel grid as auxiliary electrode and Ag/AgCl as reference one. The working electrode was the SAW sensor with a sensing area of S = 22 mm^2. All experiments were carried out at room temperature and under ambient air.

2.2.3 AFM measurements

AFM measurements were carried out, under ambient temperature, with a Nanosurf easy Scan 2 Flex AFM system in the dynamic force mode. The cantilever's resonance frequency was of about 165 kHz,

and the used probes were ACLA silicon, from AppNANO, with curvature radius of about 6 nm.

2.2.4 XPS measurements

XPS measurements were performed using a Thermo VG Scientific ESCALAB 250 system fitted with a micro-focused, monochromatic Al K_α X-ray beam (1486.6 eV, 500 µm spot size). The samples were stuck on sample holders using conductive double-sided adhesive tapes and outgassed in the fast entry airlock for at least 1 h at 5×10^{-7} mbar or better. The Avantage software, version 3.51, was used for digital acquisition and data processing. The spectra were calibrated against the C 1s main peak component C–C/C–H set at 285 eV.

2.3 Electrosynthesis of polypyrrole imprinted flumequine

Before each electrodeposition procedure, the gold sensing area of the SAW sensor was cleaned and activated by 50 µl drop of a piranha solution (98% H_2SO_4 / 30% H_2O_2 1:1 V/V), during 20 min. The substrates were then copiously rinsed with deionized double distilled water, and dried under ambient air.

All electrodeposited films were prepared in ACN solvent, as FLU is insoluble in deionized water. MIPs electropolymerization was carried out by chronoamperometry (CA) in ACN solution containing 10^{-1} M $tBuNBF_4$ and 10^{-1} M of pyrrole in presence of 10^{-2} M FLU. Thin films of non-imprinted polypyrrole polymers (NIPs) have also been prepared under the same electrodeposition conditions but without FLU.

3 DFT calculations

The gold surface was built from the optimized bulk with a cell parameter ***a*** which was found to be equal to 4.164 Å at the Perdew-Burke-Ernzerhof (PBE) level, being in good agreement with experiment (4.0782 Å)[39]. It was modeled, using Modelview software[40], as a slab representing a (111) face cut out of the optimized bulk face centered cubic cell of gold. In this approach the surface is infinite in two dimensions (in x and y directions), with a vacuum space in the z axis direction. For the slab the unit cell parameter ***a*** = 2.94 Å. The superstructure $(3\sqrt{3} \times 3\sqrt{3}\,R30)$ is used to investigate the adsorption of flumequine on the surface.

Calculations were performed in the frame of periodic DFT by means of the Vienna Ab Initio Simulation Package (VASP 5.2.11)[41-42]. The electron-ion interactions were described by the projector augmented wave (PAW)[43-44] method, representing the valence electrons, as provided in the code libraries. The convergence of the plane-wave expansion was obtained with a cut off of 500 eV. The generalized gradient approximation (GGA) was used with the functional of PBE[45-46]. The sampling in the Brillouin zone was performed on a Monkhorst–Pack grid[47] of

1 × 1 × 1 and 9 × 9 × 1 kpoints for isolated molecules and surface systems, respectively. Periodic calculations are performed in vacuum by putting them in a box such that the distance between molecules neighboring cells is around 15 Å.

The adsorption energy is calculated as the difference between complex and isolated systems relaxed individually. The most stable site adsorption energy is compared to the interaction energy between flumequine and pyrolle template.

In order to understand the selectivity of the PPy-MIP recognition layer, density functional theory (DFT) calculations were investigated to estimate the interaction energy between the matrix and either flumequine or levoflexine analytes. Quantum calculations were carried out at B3LYP/6-31+G* level of theory in both gaz phase and implicit water solvent. The latter is modelled by the polarisable continuum using Kohn Sham united atomic topologies cavities (UAKS) as implemented in Gaussian 09 software. The matrix is modelled by a pyrolle and bipyrrole in order to take into account the flexibility of the template. The two models as well as the analytes, were previously optimized and different complexes are built based intuitive knowledge on intermolecular interaction between chemical functions. The interaction energy of each complex is calculated using the formula:

$$\Delta E_{int} = E_{T-A} - (E_T + E_A) \qquad \text{(eq. 1)}$$

Where $E_{T\text{-}A}$, E_T and E_A are the optimized energies of the complex, the template and the analyte, respectively. The counterpoise methods were used to correct basis set superposition error [48].

4 Results and discussion

4.1 Electrodeposition of molecularly imprinted polypyrrole

FLU electroactivity on gold surface was tested before starting MIP electropolymerization. Analysis were performed with cyclic voltammetry, between - 0.3 and 1.5 V / Ag/AgCl, for a 10 mM FLU solution containing $tBuNBF_4$ 0.1 M/ACN. Results indicate the absence of FLU electroactivity on gold.

Fig 2a shows the CA curve relevant to the electropolymerization on the bare gold of the SH-SAW sensing area of 0.1 mol $L^{-1}$of pyrrole and 10^{-2} M of FLU in ACN solution. The continuous current decrease characterizes a blocking process on the electrode, indicating that pyrrole polymerization does not occur efficiently in the presence of FLU. Besides, only inhomogeneous black “islands” are observable on the electrode surface. This effect can be attributed to complex formation between FLU and gold which interfere with subsequent PPy electropolymerization. Similar behavior was reported previously for levofloxacin on platinum electrode[33]. In the absence of FLU, the obtained curve has the usual shape for a potentiostatic polymerization of polypyrrole (Fig 2b). It is well known [49-50] that the kinetic mechanism of film formation and growth involves different contributions: at the beginning of the experiment, the current transient decreases due to the oxidation of the adsorbed pyrrole monomers and to the simultaneous and instantaneous diffusion-controlled process which occurs at the gold electrode surface. The further rise of current is related to the continuous and gradual conductive polymer growth, which is limited by mass transfer reactions.

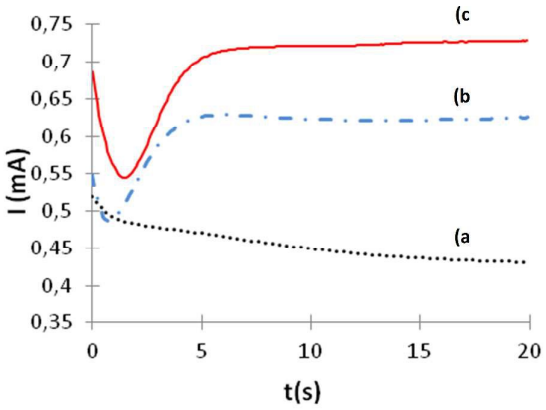

Fig 2 CA curves in ACN/tBuNBF$_4$ 0.1 mol L^{-1} solution of: (a) 10^{-1} mol L^{-1} pyrrole + 10^{-2} mol L^{-1}Flu, (b) 10^{-2} mol L^{-1} pyrrole, (c) 10^{-2} mol L^{-1} pyrrole + 10^{-3} mol L^{-1}Flu (a barrier film was firstly deposited by CA during 2 s at a constant potential of 1 V vs Ag/AgCl)

In order to prevent FLU complexes formation on the electrode surface, an easy and efficient solution consists on electrodepositing a thin polypyrrole layer which proceeds as a blocking film[31].
In this work, the barrier film was prepared by CA at a constant potential of 1 V vs Ag/AgCl during 2 s. Fig 2c shows that the anodic current of the film is slightly shifted, indicating that FLU molecules are trapped in the vicinity of the polymer matrix during the electropolymerization process. Several experiments were then performed to evaluate the appropriate electrochemical parameters (results not shown here). A molar ratio of Pyrrole/FLU equal to 10/1 was chosen for the polymer preparation.
These experimental results were confronted to quantum chemical calculations with the aim to provide additional elements about competitive interactions between PPy and FLU on one hand, and gold surface and FLU, on the other hand. The trapping energy of the flumequine in the PPy polymer was assessed at PBE level of theory as the sum of interaction energies corresponding to all possible binding sites (Fig 3).

FLU targets are trapped in the polymer matrix due to the formation of hydrogen bonds between the carbonyl oxygen atoms of FLU and N-H group of pyrrole, on one hand, and between pyrrole units and fluorine, the three tertiary amines and the carboxylic acid of FLU, on another hand.
The interaction energies per binding site are reported in Table 1. One can observe that the most stable structure corresponds to F1, for which a strong hydrogen bond is established between the amine group of pyrrole and the carbonyl group of flumequine (NH…O=C).

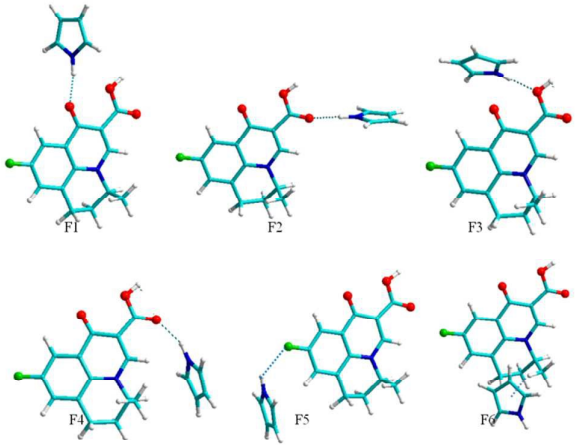

Fig 3 Interaction sites between flumequine molecule with polypyrrole and the structures of pyrrole and FLU complexes Carbon atoms are in grey; oxygen in red, nitrogen in blue, hydrogen in white and fluorine in green

The calculated interaction energy is found to be equal to - 8.36 kcal/mol. The F4 structure contains a similar hydrogen bond combined to a CH — π interaction giving an energy of interaction in a same magnitude. Surprisingly, the hydrogen bond with fluorine atom is less important with an interaction energy of -2.94 kcal/mol and a bond length of 2.45 Å. The less stable structure corresponds to F6, where the cohesion is ensured by the weak CH—π interaction. In a first approximation, we define the polymer trapping energy as the interaction energies of the sites surrounding the flumequine molecule inside a polymeric compartment.

Table 1 Interaction energies of pyrrole-FLU for the possible binding sites and the corresponding intermolecular distance (NH…X, where X= O, F and π ring of pyrrole)

Site	F1	F2	F3	F4	F5	F6
ΔE(kCal/mol)	- 8.36	- 5.39	- 5.01	- 8.13	- 2.94	- 2.07
NH….X (Å)	1.99	1.98	2.20	2.00	2.45	4.13

During the polymer formation, and in the absence of the thin barrier layer, a competition between the encapsulation of the FLU template by the PPy and its further complexation with the gold surface takes place. This last process was investigated by exploring both adsorption and physisorption sites of FLU on Au (111) surface (Fig 4). The interaction energy per site was calculated and compared to the trapping energy of FLU in the PPy polymer.

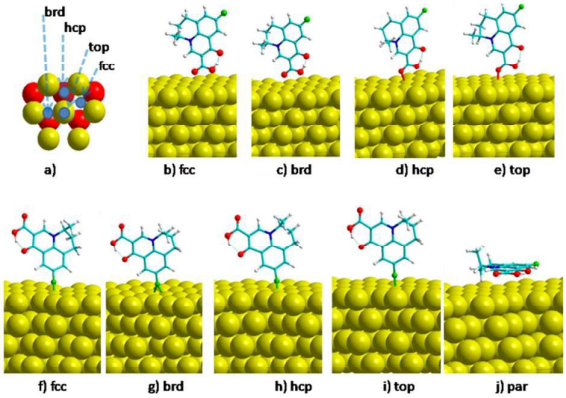

Fig 4 a) Adsorption sites labeling on Au (111) surface, the outermost layer atoms in yellow and the under layer atoms in red. The optimized structures of flumequine adsorption on Au (111) through oxygen sites (b-e) and fluorine atom(f-i). The optimized structure of flumequine physisorption on Au (j)

The adsorption of flumequine on Au (111) surface was investigated by placing the oxygen or fluorine atoms on the hollow (fcc and hcp), bridge (brd) and top position as shown on Fig 4a. The most stable adsorption site was found to be the top position in which the flumequine molecule is adsorbed through the oxygen atom. The calculated adsorption energy and the vertical spacing of the binding oxygen relative to the surface are worth -15.1 kcal/mol and 2.5 Å, respectively.

In the case of the adsorption by fluorine atom, the adsorption energies are -0.1, -3.2, -7.1 and -2.9 kcal/mol for the hcp, fcc, top and brd sites, respectively. The corresponding vertical spacing varies from 1.83 to 2.44 Å.

The flumequine physisorption is exothermic with interaction energy of -1.6 kcal/mol and an equilibrium distance of 3.06 Å. This value is probably underestimated because of the lack of van der Waals dispersion interaction that dominates in this kind of interaction.

All these results are gathered in Table 2.

Table 2 Adsorption energies (in kCal/mol) of flumequine on $(3\sqrt{3} \times 3\sqrt{3}\ R30)$ Au (111) surface and vertical spacing (in Å) of the adsorbed atom relative to the outermost layer of the surface

Adsorption site		hcp	fcc	top	brd	par
F site	ΔE (kcal/mol)	-1.6	-4.1	-7.5	-5.8	-4.6
	$d_{F\text{-}S}$ (Å)	1.83	2.09	2.28	2.07	3.06
O-site	ΔE (kcal/mol)	-12.2	-11.8	-15.1	-12.5	-
	$d_{O\text{-}S}$ (Å)	2.36	2.46	2.50	2.44	-

By comparing results presented in Tables 1 and 2; one can observe that the FLU-Au adsorption energy per site is more stable than the FLU-PPy trapping energy per site. This explains the necessity of ectrodepositing a thin polypyrrole layer before the MIP formation, a film whose main role is to block the formation of FLU-Au complexes which are favored from energetic point of view.

4.2 Extraction of flumequine

Before checking the sensing properties of the MIP, FLU molecules were extracted from the vicinity of the realized film. For this purpose, a continuous flow of a protic solution (MeOH/AcCOOH: 90/10 V/V) was pumped over the sensing area of the SAW sensor at a constant flow rate of 0.19 mL min^{-1}, using a Gilson peristaltic pump. The follow up of phase variation versus time showed an increase of phase values indicating that FLU molecules were removed from the MIP matrix by breaking the hydrogen bonds linking FLU to PPy (results not shown here).

The molecularly imprinted polymers topographies were investigated by means of atomic force microscopy before and after FLU extraction. Figs 5a and 5b (low magnification) as well as Figs 5c and 5d (high magnification) show an obvious difference between the two films, as the extracted film presents a pronounced "porous" character.

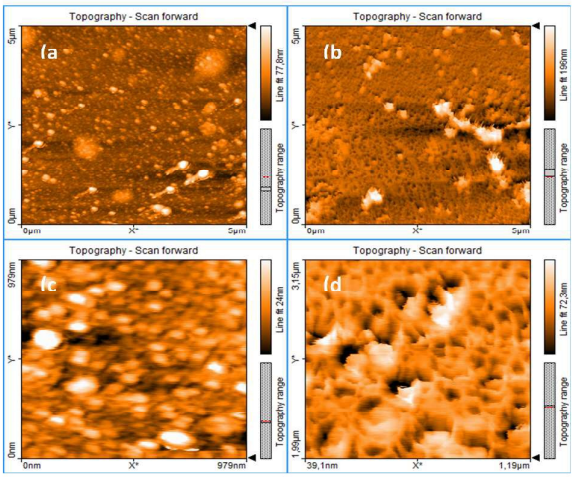

Fig 5 AFM images corresponding to the spatial frequency range $2.10^{-1} - 2.10^{2}$ μm^{-1}, for a MIP before extraction (a: 5 µm scan and c: zoom of ≈ 1 µm) and after extraction (b: 5 µm scan and d: zoom of ≈ 1 µm)

For a quantified comparison between the two surfaces, three statistical parameters were calculated (in the spatial frequency range $2.10^{-1} - 2.10^{2}$ μm^{-1}) and gathered in Table 3: the rms roughness S_q, the maximum surface peak height S_p and the maximum surface valley depth S_v.

Table 3 Rms roughness S_q, maximum surface peak height S_p and maximum surface valley depth S_v, for the MIP before and after extraction in the spatial frequency range $2.10^{-1} – 2.10^{2}$ µm^{-1}

	S_q [nm]	S_p [nm]	S_v [nm]
MIP	8.1	79	22
Extracted MIP	23.5	172	114

The increase of S_q, S_p and S_v values after FLU extraction, by factors 2.9, 2.1 and 5.2 respectively, highlights the efficiency of the extraction process to remove flumequine from their "cavities": the extracted MIP becoming rougher and the valleys deeper.

4.3 Sensing properties of the designed MIP-SAW sensor

After the extraction step, the MIP was rinsed with a solution of NaCl 0.1 M and adjusted to pH 8 with a solution of NaOH to approximate aquaculture ponds conditions. Analysis of the sensor's response indicates a quasi-linear phase variations versus flumequine concentrations until a saturation value of 10^{-4} M (Fig 6).

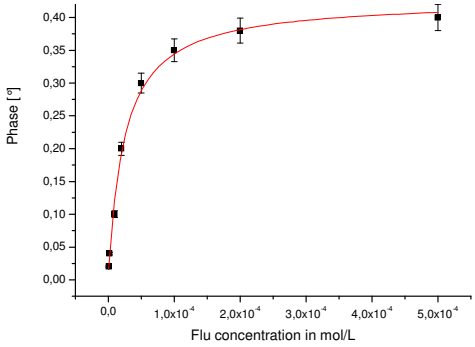

Fig 6 Phase variation versus FLU concentration

Phase shift variations (ΔΦ) versus FLU concentration (*C*) can be fitted with the "one site binding" equation:

$$\Delta\Phi = \frac{B \times C}{K + C} \qquad \text{(eq. 2)}$$

where B = 0.427 ± 0.109 ° is the maximum sensor's response to the specific binding (PPy-FLU), which is reached when flumequine molecules occupy the imprinted cavities. K = 20.00 ± 2.45 µM represents the equilibrium binding constant.

These values cannot be compared to other ones, as, to our knowledge, no studies concerning flumequine detection in an aqueous medium by a MIP have been published in the literature.

The limit of detection (LOD) of the designed MIP-SAW sensor was estimated at 1µM and the sensitivity S, calculated from the slope of the initial part of the phase/concentration curve, was found equal to 9.36 ± 0.39 °/mM.

To evaluate the possible effects of nonspecific adsorption, a 5.10^{-4} M FLU solution was injected on the sensing area of the SAW sensor coated with a non-imprinted polymer (NIP). No phase variations were recorded, but we observed some damped oscillations, which are probably due to unstable hydrogen bonds between oxygen atoms of FLU and N-H group of pyrrole (results not shown here). This indicates that the detection of an analyte by a MIP is done through two combined effects: the establishment of chemical bonds between the matrix and the molecule on one hand, and the perfect match between the molecule and the cavity, on the other hand.

Fig 7 shows the summarized values of S_p, S_q and S_v for the MIP, NIP and extracted MIP and NIP, in the spatial frequency range $2.10^{-1} – 2.10^{2}$ µm^{-1}. It is clear that the MIP presents a smoother surface than the NIP. This means that the insertion of flumequine molecules in pyrrole matrix leads to a structural rearrangement which makes the surface less rough.

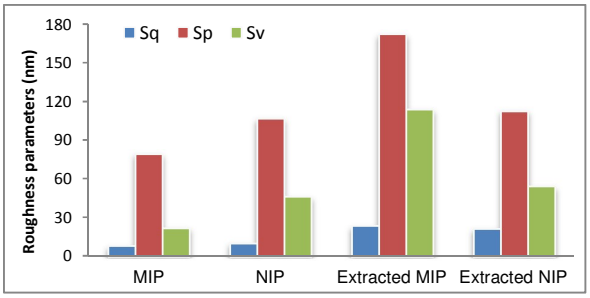

Fig 7 S_p, S_q and S_v values for the MIP, NIP and extracted MIP and NIP in the spatial frequency range $2.10^{-1} – 2.10^{2}$ µm^{-1}

Fig 7 highlights also the fact that unlike the MIP, the extraction, with a continuous flow of a protic solution, does not alter significantly the morphology of the NIP as the values of the three investigated statistical parameters remain almost constant. This confirms the fact that the chosen extraction process removes principally flumequine templates from the MIP matrix by breaking the hydrogen bonds linking FLU to PPy.

4.4 XPS characterisation

XPS was used to investigate the efficient coating of the gold substrates by polypyrrole, to assess polypyrrole doping and to track flumequine in the polypyrrole MIP with respect to the NIP.

Fig 8a displays the survey scan of the film after electrosynthesis. Its corresponding high resolution N1s region is plotted in Fig 8b. The survey region from the as-synthesized MIP has C1s, N1s and O1s regions centred at 285, 400 and 532 eV, respectively.

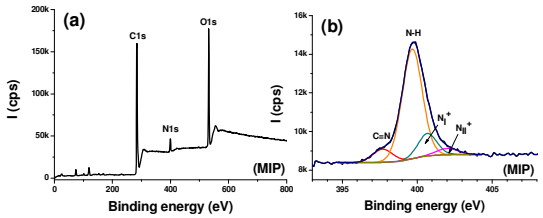

Fig 8 (a) Survey spectra of Au-MIP after synthesis; (b) high resolution N 1s region from the MIP film

No peak from the underlying gold electrode is detected indicating an efficient screening of the electrode.

The film thickness *d* was estimated from the charges transfer involved in electropolymerization process, according to the equation:

$$d = \frac{m\,Q}{n\,F\,\rho} \qquad \text{(eq. 3)}$$

Where *m* is the molecular weight of the pyrrole monomers, *Q* is the electropolymerization charge, *n* is the number of electrons involved in the polymerization processes, *F* is the Faraday's number (96500 C) and *ρ* is the polymer density[51].

d was estimated to be 400 nm which accounts for a total attenuation of the gold peak in XPS spectrum of the coated electrode.

The peaks are fitted with 4 components assigned to C=N, N-H and two positively charged nitrogen atoms noted N_I^+ and N_{II}^+, as shown in Fig 8b for the high resolution region of the MIP film before extraction of the template. Similar shapes were obtained for all samples. The surface composition of the polymer films is reported in Table 4. The latter provides the total C and O elemental percentages, and the fluorine contents coming from fluorides and flumequine. The nitrogen content is split into its 4 contributions from the imine, N-H and the two oxidized states of the nitrogen.

Table 4 Surface chemical composition of imprinted and non imprinted polypyrrole thin films (in at %)

Films	C	O	F1 (F^-)	F2 (C-F)	C=N	N-H	N_I^+	N_{II}^+	Doping level (%)[a]
MIP	72.3%	23.7%	0.03%	0.02%	0.34%	2.89%	0.54%	0.18%	18.2
$MIP_{extracted}$	71.3%	23.4	0.05%	0%	0.53%	3.52%	1.00%	0.19%	22.8
NIP	80.1%	8.83%	0.20%	0%	0.57%	8.02%	1.61%	0.66%	20.9
$NIP_{extracted}$	79.6%	9.98%	0%	0%	0.67%	7.55%	1.58%	0.61%	20.4

[a]Doping levels (in %): $D=(N_I^+ + N_{II}^+)x100\%/N$ where N the total percentage of nitrogen

The nitrogen from flumequine should have a negligibly small contribution to the total nitrogen atomic percent. The doping level was estimated from the peak fitting of the high resolution N1 regions from MIP and NIP films. For either MIP or NIP films, the doping level remains within the 18-23 % range, meaning it is relatively stable regardless imprinting or template extraction processes.

Interestingly, and despite a low atomic percent of fluorine in flumequine (3.2 %), the template molecule is detected after electrosynthesis (Fig 9a).

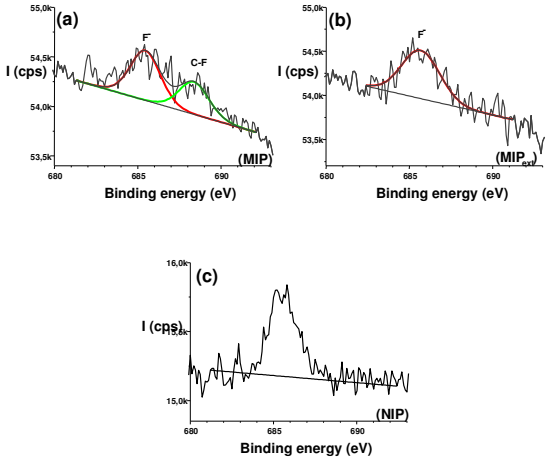

Fig 9 Peaks fitted F1s regions from (a) MIP after electrosynthesis; (b) MIP after template extraction, and (c) NIP

The F1s region is fitted with two peaks centred at 685.5 and 688.4 eV, assigned to BF_4^- and C-F corresponding to fluorine of the flumequine. This confirms that flumequine remains entrapped in the synthesised polymer. After extraction, only the low binding energy peak is persistent and the one corresponding to C-F is no longer observed (Fig 9b), indicating 0% content of fluorine from flumequine. This is strong supporting evidence for the uptake or removal of the template molecule by or from the MIP film. The recorded F1s region from the NIP (Fig 9c) shows only one peak centred at 685.5 eV which accounts for BF_4^- fluorides species.

4. 4. Selectivity test

Selectivity tests were performed with levofloxacine (LEVO), an interfering fluoroquinolone antibiotic intensively used in aquaculture ponds. Fig 10 shows that the injection of a solution of 5. 10^{-3} M of LEVO does not induce any phase shift. The oscillations, following this injection, are probably due to instable bonds, as the molecular structure of LEVO does not perfectly match to the FLU imprints. On the contrary, the injection of a solution of flumequine analyte at a concentration of 5.10^{-4}M causes a significant decrease of phase values, indicating that the functionalized cavities of the MIP were remained unoccupied after injection of LEVO and served for the specific recognition of FLU molecules.

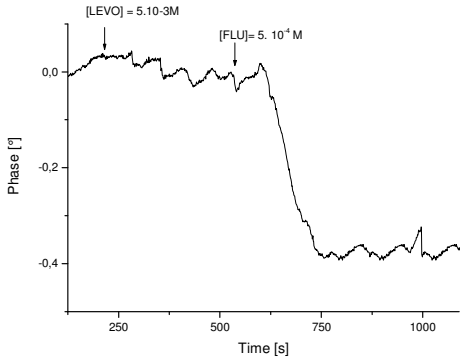

Fig 10 Gravimetric response of the SAW-MIP sensor after the injection of a solution of 5. 10^{-3} M of LEVO and a subsequent solution of 5.10^{-4} M of FLU

For each of these two analytes, we have investigated the interaction with the polymer by complexing them with one of the following oligomers: pyrrole (P), bipyrrole (BP), tripyrrole (TRP = P+ BP) and tetrapyrrole (TEP = BP+2P). All complexes were fully optimized at B3LYP/6-31+G* level of calculations in both gas and liquid phases. The molecular volumes and the total electronic energies were computed at the same level of theory. The interaction energies per volume unit of FLU and LEVO complexion with the matrix (monomer to tetramer) were deduced from the total electronic energies and molecular volumes.

The results for the most stable configurations are reported in table 3 and represented on Fig 11.

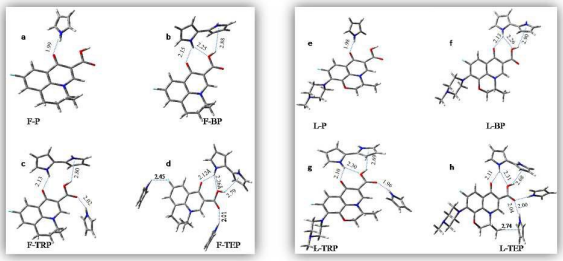

Fig 11 Most stable structures of flumequine (a-d) or levoflexacine (e-h) and the investiagted oligomers. Carbon atoms are in gray; oxygen in red, nitrogen in blue and hydrogen in white

The interaction between analytes and oligomers is characterized by the establishment of a hydrogen bond between pyrrole NH group and electronegative atoms of FLU or LEVO, and by an electrostatic interaction between the OH group of the analyte and the pyrrole π–ring.

In the case of FLU molecule the binding of the fluorine atom to the oligomers was found to be lower than that of the carbonyl group, while in the case of LEVO, the interaction with fluorine becomes more instable and the interaction with the polymer is concentrated around the carboxylic and ketone groups.

Moreover, for both FLU and LEVO, one can observe that the interaction energy decreases from the monomer to the tetramer.

Table 5 Interaction energies per unit volume (in kcal/mm^3) for the most stable complexes (in gas and water solvent) between FLU or LEVO and polymer matrix oligomers

		P	BP	TRP	TEP
FLU	gas	-163.1	-193.5	-346.9	-424.9
	water	-73.2	-83.9	-159.5	-194.1
LEVO	gas	-140.0	-163.2	-291.8	-350.2
	water	-55.6	-69.3	-129.1	-153.2

In liquid phase, the values vary from -73.2 to -194.1 kcal/mm^3 in the case of FLU and from -55.6 to -153.2 kcal/mm^3 for LEVO. The types of interaction are similar as well as the interaction energies, and the net difference in interaction energies per volume unit originates from the molecular volumes. This confirms the fact that the complementarity between a target and its further recognition cavity requires not only the establishment of chemical bonds between these two elements but also a perfect geometric concordance between them.

Conclusions

A sensitive piezoelectric chemosensor was functionalized with a thin layer of molecularly imprinted polypyrrole for the selective detection of flumequine, a fluoroquinolone antibiotic usually used in intensive aquaculture.

Electrochemical investigations and quantum chemical calculations, based on the density functional theory (DFT), highlight the necessity of electrodepositing a thin PPy blocking layer, on the gold sensing area of the SH-SAW sensor, before electropolymerizing the MIP, to prevent the formation of any Au-FLU complexes.

Flumequine template molecules were extracted from the vicinity of the MIP with a continuous flow of a protic solution (MeOH/AcCOOH: 90/10 V/V). Both AFM and XPS measurements demonstrate the efficiency of this process. The further injection of flumequine solutions causes a decrease of phase values, indicating the entrapment of the template molecules in the cavities of the MIP. Analysis of the sensor response indicates a quasi-linear phase variations versus flumequine concentrations until a saturation value of 10^{-4} M. The absence of phase shift after the injection of levofloxacine is indicative of the high selectivity of the designed sensor towards flumequine with respect to other molecules of the fluoroquinolone group.

DFT calculations showed that the interactions of the two investigated analytes with the a PPy “dense” matrix are comparable and are characterized by the establishment of a hydrogen bond between NH and electronegative atoms, and by an electrostatic OH-

π of the analyte. However, dividing the calculated energies per the volume of each molecule permits to take into account the geometrical aspect, which is one of the most important parameters involved in molecularly imprinted polymers.

This work conclusively shows that SAW sensors with thin conductive polymer sensing layers can efficiently be designed for the specific detection of flumequine. The results achieved so far pave the way to the detection of this antibiotic in real samples of water from aquacultures. More generally, the simple and versatile approach described above can be extended to molecules of relevance to veterinary, food, agricultural among other domains.

Acknowledgements

MMC wishes to thank the French ANR agency for financial support through the POLARISafe project No ANR-12-SECU-011-01.

Quantum chemical calculations were performed using HPC resources from GENCI - [CCRT/CINES/IDRIS] (Grant 2015-[c2015087006]).

Note

Electrochemical and gravimetric results are part of the project BIOVecQ (PS1.3_08) funded by the Cross-Border Cooperation Programme Italy–Tunisia in the frame of the European Neighbourhood and Partnership Instrument IEVP-2007-2013

References

1. F. C. Cabello, *Environ. Microbiol*., 2006, **8**, 1137-1144.
2. S. Calvez, H. Gantelet, G. Blanc, D.-G. Douet and P. Daniel, *Dis. Aquat. Org.*, 2014, **109**, 117-126.
3. T. X. Le, Y. Munekage and S.-i. Kato, *Sci. Total Environ.*, 2005, **349**, 95-105
4. C. Scarano, C. Spanu, G. Ziino, F. Pedonese, A. Dalmasso, V. Spanu, S. Virdis and E. De Santis, *New Microbiol.* 2014, **37**, 329-337.
5. H. Hektoen, J. A. Berge, V. Hormazabal and M. Yndestad, *Aquaculture*, 1995, **133**, 175-184.
6. M. Naviner, L. Gordon, E. Giraud, M. Denis, C. Mangion, H. Le Bris and J.-P. Ganiere, *Aquaculture*, 2011, **315**, 236-241.
7. M. Touraki, I. Niopas, E. Ladoukakis and V. Karagiannis, *Aquaculture*, 2010, **306**, 146-152.
8. A. Rusu, G. Hancu and V. Uivaroşi, *Environ Chem Lett*, 2015, **13,** 21-36.
9. M. Sturini, A. Speltini, L. Pretali, E. Fasani and A. Profumo, *J. Sep. Sci.*, 2009, **32**, 3020-3028.
10. A. Rúbies, E. Muñoz, D. Gibert, N. Cortés-Francisco, M. Granados, J. Caixach and F. Centrich, *J. Chromatogr. A*, 2015, **1386**, 62-73.
11. M. E. Dasenaki and N. S. Thomaidis, *Anal. Chim. Acta*, 2015, DOI: http://dx.doi.org/10.1016/j.aca.2015.04.013.
12. X.-k. OuYang, Y.-Y. Luo, Z.-S. Wen, W.-J. Wu, G.-Z. Cao, X.-Y. Zhu, L.-y. Yang, Y.-G. Wang and J.-Y. Dong, *Food Anal. Meth*., 2014, **7**, 1770-1775.
13. M. Lombardo-Agüí, A. M. García-Campaña, C. Cruces-Blanco and L. Gámiz-Gracia, *Food Control*, 2015, **50**, 864-868.
14. N. Stoilova, A. Surleva and G. Stoev, *Food Anal. Meth*, 2013, **6**, 803-813.
15. E. Turiel, A. MartÃ-n-Esteban and J. L. Tadeo, *Anal. Chim. Acta*, 2006, **562**, 30-35.
16. J. F. Lawrence, *Chromatographia*, 1987, **24**, 45-50.
17. I. A. Shanin, N. T. D. Thuy and S. A. Eremin, *Moscow Univ. Chem. Bull.*, 2014, **69**, 136-141.
18. X. Tao, M. Chen, H. Jiang, J. Shen, Z. Wang, X. Wang, X. Wu and K. Wen, *Anal. Bioanal. Chem*., 2013, **405**, 7477-7484.
19. L. Okerman, H. Noppe, V. Cornet and L. De Zutter, *Food Addit. Contam*., 2007, **24**, 252-257.
20. S. Weigel, M. G. Pikkemaat, J. W. A. Elferink, P. P. J. Mulder, A.-C. Huet, P. Delahaut, S. Schittko, R. Flerus and M. Nielen, *Food Addit. Contam*. *A*, 2009, **26**, 441-452.
21. A. C. Huet, C. Charlier, S. Weigel, S. B. Godefroy and P. Delahaut, *Food Addit. Contam*. *A* 2009, **26**, 1341-1347.
22. Y. Lattach, N. Fourati, C. Zerrouki, J.-M. Fougnion, F. Garnier, C. Pernelle and S. Remita, *Electrochim. Acta*, 2012, **73**, 36-44.
23. N. Fourati, M. Seydou, C. Zerrouki, A. Singh, S. Samanta, F. Maurel, D. K. Aswal and M. Chehimi, *ACS Appl. Mater. Interfaces*, 2014, **6**, 22378-22386.
24. Y. Bergaoui, C. Zerrouki, N. Fourati, J.M. Fougnion, A. Abdelghani, *Eur. Phys. J. Appl. Phys*., 2011, **56**, 13705- 13709.
25. K. Haupt, A. Linares, M. Bompart and B. Bui, in Molecular Imprinting, ed. K. Haupt, Springer Berlin Heidelberg, 2012, vol. 325, ch. 307, pp. 1-28.
26. I. A. Nicholls, B. C. G. Karlsson, G. D. Olsson and A. M. Rosengren, *Ind. Eng. Chem. Res.* 2013, **52**, 13900-13909.
27. A. Mirmohseni, M. Shojaei and R. Pourata, *RSC Adv.*, 2014, **4**, 20177-20184.
28. R. H. Chasta and R. N. Goyal, *Talanta*, 2014, **125**, 167-173.
29. L. Uzun and A. P. F. Turner, *Biosens. Bioelectron.*, 2015, http://dx.doi.org/10.1016/j.bios.2015.07.013i
30. C.-H. Weng, W.-M. Yeh, K.-C. Ho and G.-B. Lee, *Sens. Actuat. B: Chem*., 2007, **121**, 576-582.
31. N. Maouche, M. Guergouri, S. Gam-Derouich, M. Jouini, B. Nessark and M. M. Chehimi, *J. Electroanal. Chem*., 2012, **685**, 21-27.
32. A. Ramanavičius, A. Ramanavičienė and A. Malinauskas, *Electrochim. Acta*, 2006, **51**, 6025-6037.
33. E. Mazzotta, C. Malitesta, M. Dïaz-Älvarez and A. Martin-Esteban, *Thin Solid Films*, 2012, **520**, 1938-1943.
34. T.-C. Tsai, H.-Z. Han, C.-C. Cheng, L.-C. Chen, H.-C. Chang and J.-J. J. Chen, *Sens. Actuat. B: Chem*., 2012, **171-172**, 93-101.
35. T. Qian, C. Yu, X. Zhou, P. Ma, S. Wu, L. Xu and J. Shen, *Biosens. Bioelectron*, 2014, **58**, 237-241.
36. H. Okuno, T. Kitano, H. Yakabe, M. Kishimoto, H. Siigi and T. Nagaoka, *Anal. Chem.*, 2002, **74**, 4184-4190.
37. M. Rueping, M. Stoeckel, E. Sugiono, T. Theissmann, *Tetrahedron*, 2010, **66**, 6565-6568.

38. M. Naeem and K. K. S. Rafiq, *J. App. Sci*, 2006, 6, 373-379
39. A. Maeland and T. B. Flanagan, *Can. J. Phys.*, 1964, **42**, 2364-2366.
40. http://www.enscp.fr/labos/LPCS/MRS/Modelview.
41. G.Kresse and J. Hafner, *Phys. Rev. B* 1993, **47**, 558-561.
42. G.Kresse and J. Hafner, *Phys. Rev. B* 1994, 49, 14251-14269.
43. P. E. Blochl, *Phys. Rev. B* 1994, 50, 17953-17979.
44. G. Kresse and D. Joubert, *Phys. Rev. B* 1999, 59, 1758-1775.
45. B. Hammer, L. B. Hansen, J. K. Norskov, *Phys. Rev. B* 1999, 59, 7413-7421.
46. J. P. Perdew, K. Burke, M. Ernzerhof, *Phys. Rev. Lett.* 1997, 78, 1396 (E).
47. H. J. Monkhorst and J. D. Pack, *Phys. Rev. B*, 1976, **13**, 5188-5192.
48. Boys, S.F. and F. Bernardi,. *Mol. Phys.*, 1970, **19**, 553-566.
49. L. H. Mendoza-Huizar, J. Robles and M. Palomar-Pardavé, *J. Electroanal. Chem*., 2003, **545**, 39-45.
50. M. F. Suarez-Herrera and J. M. Feliu, *Phys. Chem. Chem. Phys.*, 2008, **10**, 7022-7030.
51. L.T.Panasyuk, V.M.Mirsky, A.S.Piletsky, O.S. Wolfbeis, *Anal. Chem.*, 1999, **71**, 4609-4613.

